Defect and Diffusion Forum
ISSN: 1662-9507, Vol. 426, pp 57-64
doi:10.4028/p-h6l351

Submitted: 2022-09-04
Revised: 2022-11-23
Accepted: 2022-11-25
Online: 2023-06-06

Effective Penetration Depth Investigation for Frank Type Dislocation (Deflected TSDs/TMDs) on Grazing Incidence Synchrotron X-Ray Topographs of 4H-SiC Wafers

Qianyu Cheng[1,a*], Hongyu Peng[1,b], Zeyu Chen[1,c], Shanshan Hu[1,d], Yafei Liu[1,e], Balaji Raghothamachar[1,f] and Michael Dudley[1,g]

[1]Department of Materials Science and Chemical Engineering, Stony Brook University, Stony Brook, NY, USA

[a]qianyu.cheng@stonybrook.edu, [b]hongyu.peng@stonybrook.edu, [c]zeyu.chen@stonybrook.edu, [d]shanshan.hu@stonybrook.edu, [e]yafei.liu@stonybrook.edu, [f]balaji.raghothamachar@stonybrook.edu, [g]michael.dudley@stonybrook.edu

Keywords: 4H-SiC, X-ray topography, ray-tracing simulation, penetration depth, frank type dislocation, deflected TSD/TMD

Abstract. In 4H-SiC crystals, Frank type dislocations are created through the deflection of threading screw/mixed dislocations onto the basal plane. Grazing-incidence X-ray topographs are often used to evaluate the density of such dislocations and a knowledge of the effective penetration depth is therefore essential. In this study, a systematic analysis is performed to investigate the effective penetration depth, which is the depth from which contrast from the dislocation is still discernible. This is achieved by comparison between observed topographic images and detailed ray tracing simulations. Simulations shows no significant contrast difference between a deflected TSD and a deflected TMD with the same line direction since the large ***c*** component is the dominant contributor to the effective misorientation, whereas the effect of ***a*** component is rather negligible. Therefore, this effective penetration depth study uses ray tracing simulation images of deflected TSDs with photoelectric absorption applied to compare with all topographically observed Frank type dislocations. Analysis first reveals that the effective penetration depth varies with the angle between the off-cut direction and the line direction of a Frank type dislocation, and the effective penetration depth is significantly deeper compared to that of a BPD. Further, the effective penetration depth on ray tracing simulations with absorption applied matches well with experimentally measured depth. The study also evaluated the effectiveness of a simplified model based on an approximate expression for the effective misorientation of a dislocation modulated by photoelectric absorption. This was also found to yield satisfactory results and can be used as a universal method to determine the effective penetration depth for Frank type dislocations with ***c*** component of Burgers vector.

Introduction

The demand for power electronic devices fabricated from silicon carbide (SiC) has increased rapidly in recent years for a diverse range of existing and emerging applications. The development of device technology highly depends on the quality of substrate and epitaxial material and the number of deleterious defects within, as those are critical factors that impact the device performance and long-term reliability [1, 2]. However, various defects within the SiC crystal can degrade the device performance. Frank type dislocations, also known as deflected threading screw/mixed dislocations (TSDs/TMDs), are considered as particularly deleterious as extensive studies revealed the formation of Frank stacking faults (SFs) and Shockley-Frank SFs associated with deflected TSDs and deflected TMDs by the overgrowth of macro-steps during the crystal growth process [3-5], which can further lead to negative impact on the reverse characteristics of p-n and Schottky diodes with increased reverse leakage current [6]. Therefore, understanding the nature of Frank type dislocations (deflected TSDs/TMDs) is of great importance for preventing the degradation or premature breakdown of devices.

Synchrotron X-ray topography (XRT) in grazing-incidence geometry is commonly employed for detailed analysis of 4H-SiC wafers with 4° off-cut, meaning the basal plane is tilted 4° from the wafer surface along the $[11\bar{2}0]$. direction. This geometry is particularly powerful to study dislocations lying on the basal plane as information on defects from within the effective penetration depth of X-rays is exclusively revealed. Previous study by Q. Cheng et al. [7] has established a comprehensive procedure to define this effective penetration depth for basal plane dislocations (BPDs) through analyzing the topographic contrast of BPDs with different Burgers vector and line direction combinations in conjunction with ray tracing simulations. Study indicates the effective penetration depth is not a fixed value but associated with the observable contrast of an individual dislocation, which is related to the effective misorientation of the dislocation modulated by the photoelectric absorption effect. The effective penetration depth range of BPDs calculated through the simplified model developed in that study is around 6.0~17.4 μm. However, Frank type dislocations normally have much longer observable length on the topograph compared to BPDs as shown in Fig. 1, suggesting the operating penetration depths are different from BPDs. Therefore, further investigation is required to enable three-dimensional Frank type dislocation configuration analysis.

In this study, the effective penetration depth study is conducted on Frank type dislocations with different Burgers vector and line direction combinations in physical vapor transport (PVT) grown 4° off-axis 4H-SiC crystals. Frank type dislocations were revealed by synchrotron X-ray grazing-incidence topography using the $11\bar{2}8$ reflection. The dislocation nature of such Frank type dislocations observed topographically were confirmed by ray tracing simulations [8] that incorporates the effects of surface relaxation [9] and photoelectric absorption [10, 11]. Ray tracing simulation is an effective approach that has been proven capable for characterizing dislocations in various crystals [12-16]. Its principle is based on the orientation contrast mechanism [17], where the dislocation image is simulated by calculating the direction of local diffracted X-ray beams and projecting the diffracted X-rays onto the recording plate. The local misorientation of the lattice planes associated with the presence of a dislocation is subsequently revealed as dark or white contrast differences due to the superimposition or separation of diffracted X-rays, which induce inhomogeneous intensity distributions. The simplified model developed based on the full ray tracing simulation approach to estimate the effective misorientation and corresponding effective penetration depth of a dislocation [7] is applied for Frank type dislocations in this study to verify its effectiveness.

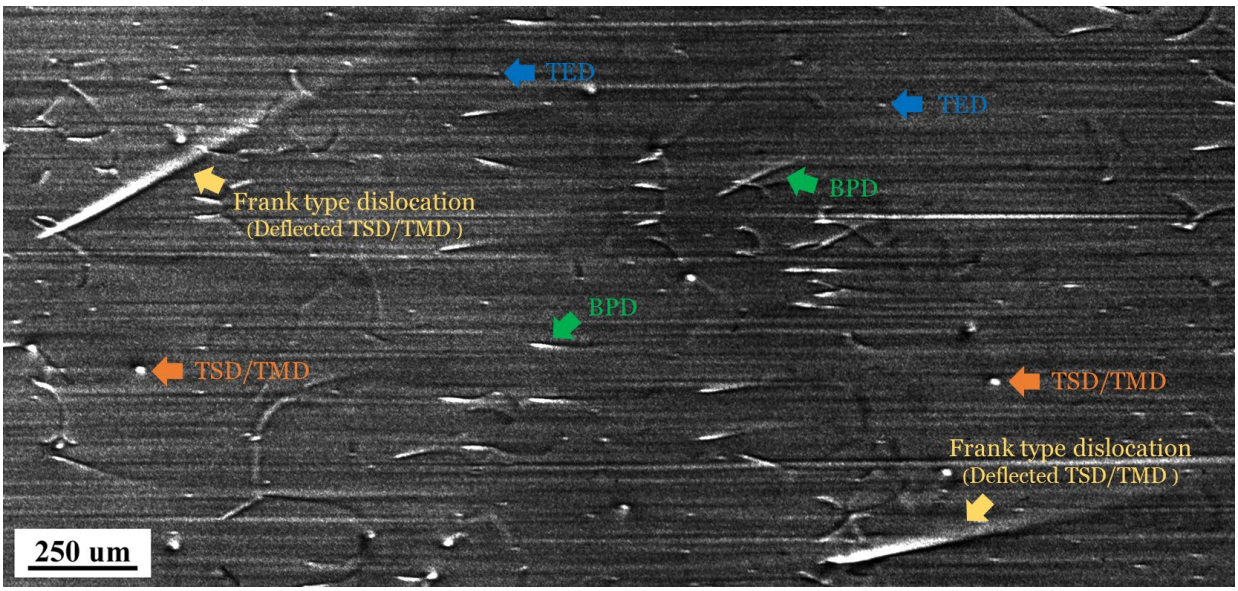

Fig. 1: Grazing-incidence synchrotron monochromatic beam X-ray topograph recorded from a 4H-SiC substrate wafer in $11\bar{2}8$ reflection showing the contrast configuration of different types of dislocations.

Experiment

Synchrotron monochromatic beam X-ray topography experiment were conducted in grazing-incident geometry for 4° off-axis 4H-SiC substrate wafers grown by PVT. $11\bar{2}8$ reflection topographs were recorded from the Si-face of the specimen at an energy of 8.99 keV. X-ray topography images were recorded on Agfa Structurix D3-SC films with approximately 1 μm resolution. The experiment was carried out at Beamline 1-BM of the Advanced Photon Source (APS) in Argonne National Laboratory (ANL). The length of dislocations on both topographs and simulation images are measured from the end of the contrast feature observed at the surface intersection down to the position where the gray value intensity of the dislocation contrast decreases to 1/10 of the maximum, measured using ImageJ [18].

The dislocation contrast observed on the topograph is studied in conjunction with ray tracing simulation. The simulation assumes rays contributing to the dislocation image do not undergo extinction but only absorption [19, 20]. Therefore, ray tracing simulation was performed at different depths below the surface subjecting each such set of diffracted beams to photoelectric absorption. This process is repeated until the dislocation contrast is no longer discernible. The completed simulated dislocation image is generated by stacking all the images from different depths below the surface [10, 11]. Ray tracing simulations were run on personal computers using Jupyter Notebook 6.1.4.

Results and Discussion

Frank type dislocations are created through the deflection of threading screw or mixed dislocations. During 4H-SiC growth process, the outcrops associated with TSDs or TMDs can be overgrown by macro-steps, which consequently deflect the threading dislocations that were originally propagating approximately along the $[000\bar{1}]$ growth axis onto the basal plane (Fig. 2 (a)). The deflected TSDs or TMDs have their line directions following the step flow direction, until it meets steps moving in the opposite direction (from for example a screw dislocation spiral source) that can possibly redirect them back into the growth direction (Fig. 2 (b-c)).

The misorientation field around a dislocation is represented by the deviation from the perfect Bragg angle δθ ($\delta\theta = \theta - \theta_B$, θ is the angle between the incident X-rays and the diffraction plane, θ_B is the Bragg anle) [21]. Compared to the misorientation field of a BPD (Fig. 3 (a)), the misorientation fields of Frank type dislocations (Fig. 3 (b) for deflected TSD and Fig. 3 (c) for deflected (TMD)) are signifcantly larger and therefore, observable dislocation contrasts are correspondingly larger (see Fig. 1). Between the two types of Frank type dislocations, however, the difference in the magnitude of the misorientation fields is slight since the large $\boldsymbol{c}$ component is the dominant contributor to the effective misorientation in both cases. This effect is demonstrated by comparing the ray tracing simulated images of right-handed Frank type dislocations with the same line direction but different Burgers vectors (Fig. 4). No distinct dislocation contrast configuration variation is observed between the simulations of a deflected TSD and a deflected TMD. Therefore, the effective penetration depth study of Frank type dislocations can be achieved by simply using ray tracing simulation images of deflected TSDs with $\boldsymbol{c}$ component of Burgers vector to compare with all topographically observed Frank type dislocations.

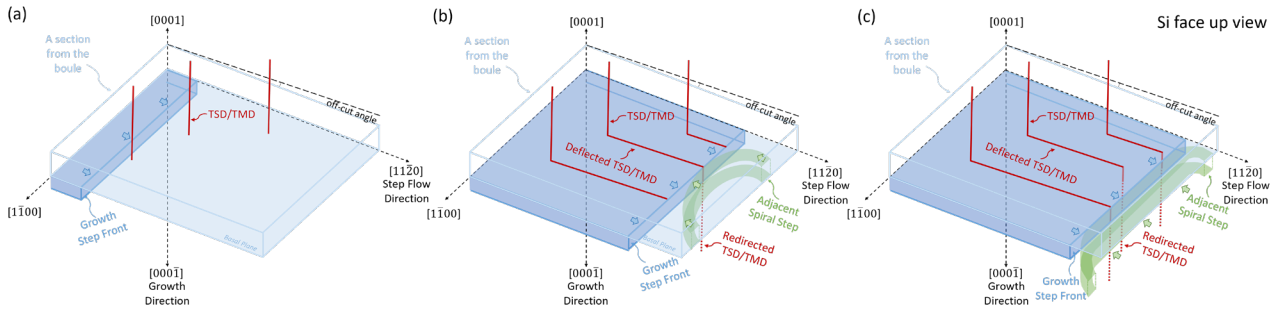

Fig. 2: Schematic diagram of Frank type dislocation formation in a section from the boule during the growth process viewed as Si face up. TSDs/TMDs grown toward the carbon face along the growth direction encounter the growth step front (a); the overgrowth of surface outcrops of TSDs/TMDs by macro-steps deflect them onto the basal plane (b); deflected TSDs/TMDs redirected back to threading orientation after meeting an adjacent step (c).

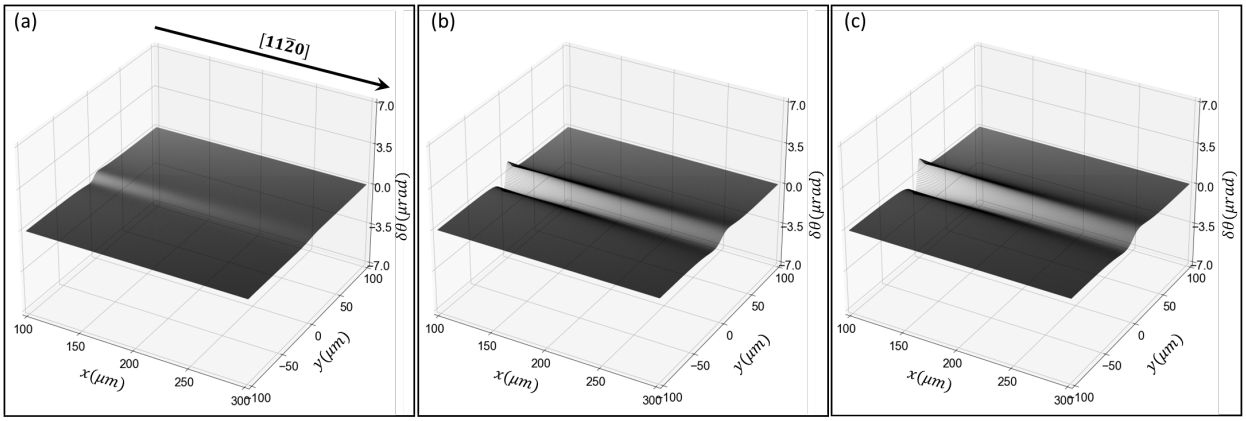

Fig. 3: Misorientation field at the surface of the sample generated by a screw-type BPD with Burgers vector $b = \frac{1}{3}[11\bar{2}0]$ (a); a deflected TSD with Burgers vector $b = [000\bar{1}]$ (b); a deflected TMD with Burgers vector $b = \frac{1}{3}[11\bar{2}\bar{3}]$.

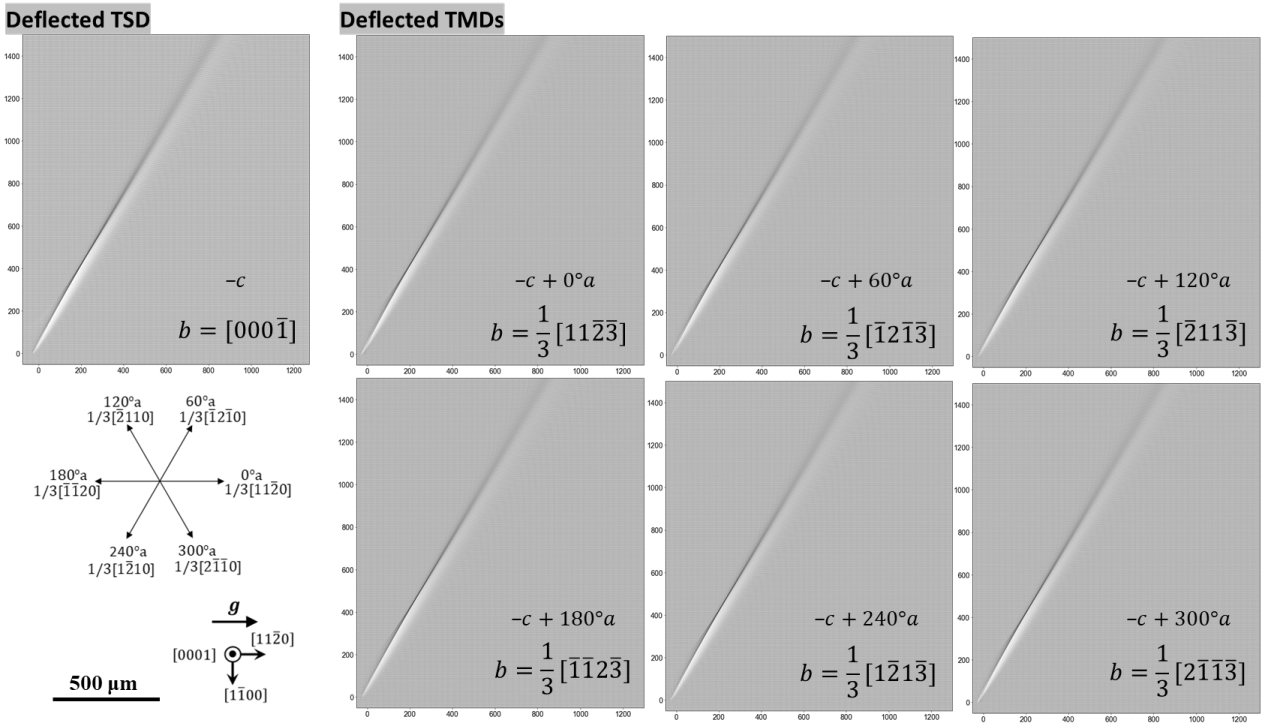

Fig. 4: Ray-tracing simulated contrasts of right-handed deflected TSD and deflected TMDs with different Burgers vector combinations under the same line direction $\varphi = 30°$ (30° clockwise to $[\bar{1}100]$).

The effective penetration depth t of a dislocation lying on the basal plane can be calculated based on its observable dislocation contrast through Eq. 1 [7]:

$$t = \mathrm{L} \times \tan 4^{\circ}. \quad (1)$$

where L is the projected length of a dislocation measured along the 4° off-cut direction of its observable length.

Fig. 5 gives four sets of examples of Frank type dislocations observed on topographs with $\pm \boldsymbol{c}$ Burgers vector and different line directions. The projected lengths measured from each dislocation are 834 μm (Fig. 5 (a-2)), 763 μm (Fig. 5 (c)), 683 μm (Fig. 5 (e)), and 848 μm (Fig. 5 (g)), corresponding to effective penetration depths of 58.3 μm, 53.4 μm, 47.8 μm, and 59.3 μm, respectively. These results are compared with corresponding ray tracing simulation images shown in Fig. 5 (b), Fig. 5 (d), Fig. 5 (f), and Fig. 5 (h). Both the dislocation contrast configurations and projected lengths match within reasonable range (≤ 6% deviation), again confirming that ray tracing simulation method with photoelectric absorption incorporated is effective in simulating these images. Analysis clearly indicates that the effective penetration depth varies with the direction of Frank type dislocations, similar to that observed for BPDs [7]. Note the shorter length of Frank type dislocation marked 1 in Fig. 5(a). The much shorter projected length does not match the expected value obtained through ray tracing simulation or the approximate value from the simplified model (discussed later). Its sudden contrast interruption and termination indicates that this dislocation was likely redirected back into a TSD/TMD along the c-axis. The redirection point is estimated at a depth around 25.7 μm away from the surface.

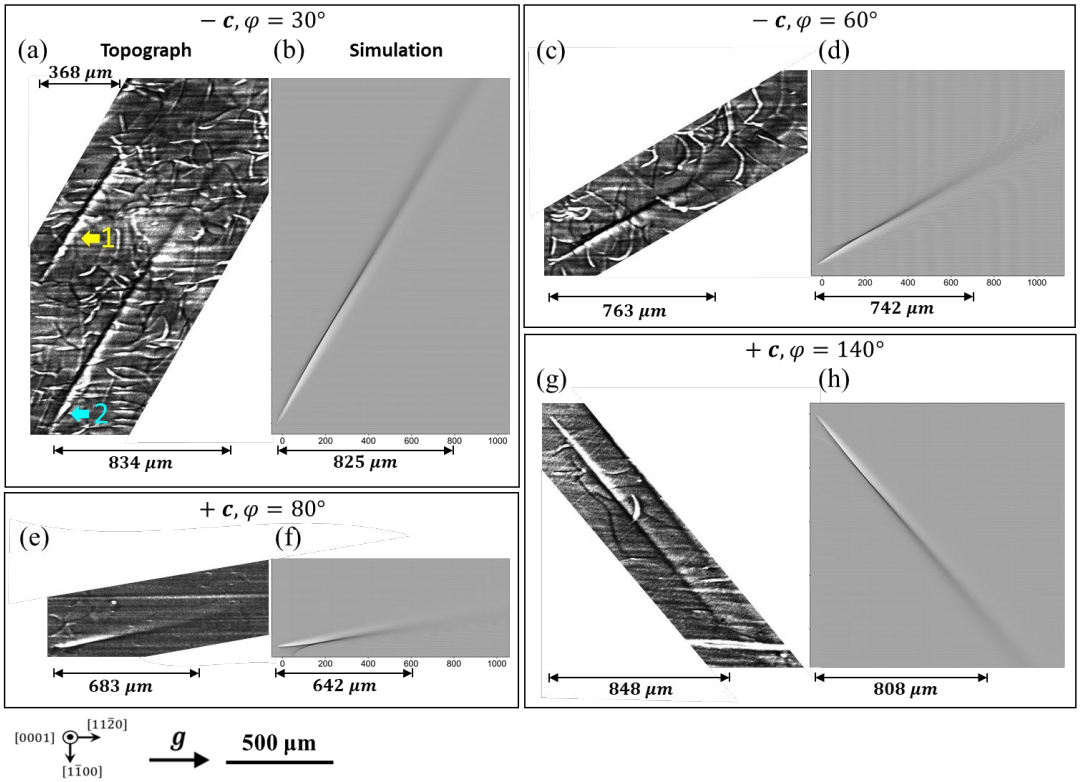

Fig. 5: $11\bar{2}8$ Grazing-incidence X-ray topographs of Frank type dislocations with line direction of $\varphi = 30^{\circ}$ (a); $\varphi = 60^{\circ}$ (c); $\varphi = 80^{\circ}$ (e); and $\varphi = 140^{\circ}$ (g), with corresponding ray-tracing simulation results (b), (d), (f), and (g), respectively. The line direction φ is defined as the angle clockwise to $[\bar{1}100]$.

To provide an alternative approach assessing the effective penetration depth of a dislocation lying on the basal plane intended for those without the access to ray tracing simulation, a simplified model

based on an approximate expression for the effective misorientation $\Delta\theta$ associated with the dislocation modulated by the photoelectric absorption effect has been developed [7]:

$$t = t_0 \cdot c\Delta\theta. \quad (2)$$

$$t_0 = \frac{\ln 10}{\mu(\frac{1}{\sin\alpha_0}+\frac{1}{\sin\alpha_h})}. \quad (3)$$

$$\Delta\theta = |\boldsymbol{g}\cdot\boldsymbol{b_s}| + |\boldsymbol{g}\cdot\boldsymbol{b_e}| + \left|(\frac{1}{\pi(1-\nu)})(\boldsymbol{g}\cdot(\boldsymbol{b_e}\times\boldsymbol{l}))\right|. \quad (4)$$

$$\boldsymbol{b_s} = (\boldsymbol{b}\cdot\boldsymbol{l})\boldsymbol{l}. \quad (5)$$

$$\boldsymbol{b_e} = \boldsymbol{b}\times\boldsymbol{l}\times\boldsymbol{l}. \quad (6)$$

where t_0 is the penetration depth of X-rays calculated from photoelectric absorption, μ is the linear absorption coefficient, α_0 is the incident angle and α_h is the exit angle with the surface. c is a constant with an average value around 0.87 obtained through the full ray tracing simulation approach with systematic analysis. $\boldsymbol{g}$ is the diffraction vector, $\boldsymbol{b}$ is the Burgers vector, $\boldsymbol{l}$ is the line direction, $\boldsymbol{b_s}$ and $\boldsymbol{b_e}$ represent the screw and edge components of the Burgers vector, respectively, and ν is the Poisson ratio.

This simplified model has been shown to be work well for estimating the effective penetration depths of BPDs [7] and is also proved applicable for Frank type dislocations as shown in Table 1. Table 1 summarizes the effective penetration depths and theoretical projected lengths calculated through the simplified model for Frank type dislocations in the same Burgers vector and line direction as the ones observed in Fig. 5, and compares it with the results obtained topographically and through simulation. The full ray tracing simulation and the simplified model values are within 6% of the experimental values, indicating either approach may be useful for penetration depth analysis.

The effective penetration depth range of Frank type dislocations with $\boldsymbol{c}$ component of Burgers vector at line directions from $\varphi = 20°$ to $\varphi = 160°$ are estimated as 42.5~60.1 μm according to full ray tracing simulation. This result is comparable to the 46.3~60.8 μm effective penetration depth range of deflected TSDs obtain through the simplified model. Both approaches reveal the shallowest effective penetration depth for a deflected TSD is observed when the line direction is parallel to the off-cut $[11\bar{2}0]$ direction (i.e., $\varphi = 90°$). Effective penetration depth gradually increases as the angle between the line direction and $[11\bar{2}0]$ increases, until the deepest effective penetration depth is reached at $\varphi = 20°$ and $\varphi = 160°$.

Table 1: Results of Effective Penetration Depth Study for Frank Type Dislocations obtained through Different Methods

Dislocation in Fig. 5	Burgers Vector	Line Direction		Methods		
				Topograph Measurement	Simulation Measurement	Simplified Model Estimation
a-2	- $\boldsymbol{c}$	30°	Projected Length (μm)	834	825	853
			Effective Penetration Depth (μm)	58.3	57.7	59.6
c	- $\boldsymbol{c}$	60°	Projected Length (μm)	763	742	773
			Effective Penetration Depth (μm)	53.4	51.9	54.0
e	+ $\boldsymbol{c}$	80°	Projected Length (μm)	683	642	701
			Effective Penetration Depth (μm)	47.8	44.9	49.0
g	+ $\boldsymbol{c}$	140°	Projected Length (μm)	848	808	831
			Effective Penetration Depth (μm)	59.3	56.5	58.1

Summary

This study investigated the effective penetration depth of Frank type dislocations in grazing-incidence monochromatic beam X-ray topographs in 4° off-cut 4H-SiC wafers in conjunction with ray tracing simulation incorporating the effects of both surface relaxation and absorption. Study concentrated on deflected TSDs with ***c*** component of Burgers vector since the effective misorientation associated with ***a*** component is less significant as revealed by ray tracing simulation, which leads to negligible contrast configuration difference between a deflected TSD and a deflected TMD. Quantitative analysis was performed on Frank type dislocations with ± ***c*** Burgers vector and different line directions by comparing topographically observed dislocation features with simulation images. The effective penetration depths predicted by the ray tracing simulation with absorption effects incorporated matches well with experimentally measured depths for Frank type dislocations of different line directions. Study revealed Frank type dislocations with significantly deeper effective penetration depth compared to BPDs. Effective penetration depth variation is found associated with the angle between off-cut direction and the line direction of Frank type dislocations. A simplified model based on the approximate expression of effective misorientation associated with a dislocation modulated by the photoelectric absorption effect is proven effective to estimate the effective penetration depth for a Frank type dislocation. This simplified model can be used as an alternative method to the full ray tracing simulation approach.

References

[1] H. Das, S. Sunkari, J. Justice, H. Pham, K.S. Park, Effect of defects in silicon carbide epitaxial layers on yield and reliability, Mater. Sci. Forum 963 (2019) 284-287.

[2] T. Kimoto, A. Iijima, H. Tsuchida, T. Miyazawa, T. Tawara, A. Otsuki, T. Kato, Y. Yonezawa, Understanding and reduction of degradation phenomena in SiC power devices, 2017 IEEE International Reliability Physics Symposium (IRPS) (2017) 2A-1.1-2A-1.7.

[3] M. Dudley, F. Wu, H. Wang, S. Byrappa, B. Raghothamachar, G. Choi, S. Sun, E.K. Sanchez, D. Hansen, R. Drachev, S.G. Mueller, M.J. Loboda, Stacking faults created by the combined deflection of threading dislocations of Burgers vector c and c+a during the physical vapor transport growth of 4H–SiC, Appl. Phys. Lett. 98 (2011) 232110..

[4] F.Z. Wu, M. Dudley, H.H. Wang, S.Y. Byrappa, B. Raghothamachar, E. Sanchez, G.Y. Chung, D.M. Hansen, S.G. Mueller, M.J. Loboda, The Nucleation and Propagation of Threading Dislocations with C-Component of Burgers Vector in PVT-Grown 4H-SiC, Mater. Sci. Forum 740-742 (2013) 217-220.

[5] M. Dudley, H.H. Wang, F.Z. Wu, S.Y. Byrappa, B. Raghothamachar, G. Choi, E. Sanchez, D.M. Hansen, R. Drachev, S.G. Mueller, M.J. Loboda, Formation Mechanism of Stacking Faults in PVT 4H-SiC Created by Deflection of Threading Dislocations with Burgers Vector c+a, Mater. Sci. Forum, 679-680 (2011) 269-272.

[6] H. Tsuchida, M. Ito, I. Kamata, M. Nagano, Formation of extended defects in 4H-SiC epitaxial growth and development of a fast growth technique, Phys. Status Solidi B 246 (2009) 1553-1568.

[7] Q.Y. Cheng, H.Y. Peng, S.S. Hu, Z.Y. Chen, Y.F. Liu, Ray-Tracing Simulation Analysis of Effective Penetration Depths on Grazing Incidence Synchrotron X-Ray Topographic Images of Basal Plane Dislocations in 4H-SiC Wafers, Mater. Sci. Forum 1062 (2022) 366-370.

[8] X.R. Huang, M. Dudley, W.M. Vetter, W. Huang, W. Si, C.H. Carter Jr, Superscrew dislocation contrast on synchrotron white-beam topographs: an accurate description of the direct dislocation image, J. Appl. Cryst. 32 (1999) 516-524.

[9] H. Peng, T. Ailihumaer, F. Fujie, Z. Chen, B. Raghothamachar, and M. Dudley, Influence of surface relaxation on the contrast of threading edge dislocations in synchrotron X-ray topographs under the condition of g . b = 0 and g . b x l = 0, J. Appl. Cryst. 54 (2021) 439-443.

[10] F. Fujie, H. Peng, T. Ailihumaer, B. Raghothamachar, M. Dudley, S. Harada, M. Tagawa, and T. Ujihara, Synchrotron X-ray topographic image contrast variation of screw-type basal plane dislocations located at different depths below the crystal surface in 4H-SiC, Acta Mater. 208 (2021) 116746.

[11] T. Ailihumaer, H. Peng, F. Fujie, B. Raghothamachar, M. Dudley, S. Harada, and T. Ujihara, Surface relaxation and photoelectric absorption effects on synchrotron X-ray topographic images of dislocations lying on the basal plane in off-axis 4H-SiC crystals, Mater. Sci. Eng.: B 271 (2021) 115281.

[12] J. Guo, Y. Yang, F. Wu, J. Sumakeris, R. Leonard, O. Goue, B. Raghothamachar, M. Dudley, Direct Determination of Burgers Vectors of Threading Mixed Dislocations in 4H-SiC Grown by PVT Method, J. Electron. Mater. 45 (2016) 2045-2050.

[13] Q. Cheng, T. Ailihumaer, Y. Liu, H. Peng, Z. Chen, B. Raghothamachar, M. Dudley, Characterization of Dislocations in 6H-SiC Wafer Through X-Ray Topography and Ray-Tracing Simulations, J. Electron. Mater. 50 (2021) 4104-4117.

[14] T. Ailihumaer, H. Peng, Y. Liu, Q. Cheng, Z. Chen, S. Hu, B. Raghothamachar, M. Dudley, Analysis of Dislocation Contrast in Synchrotron Grazing-incidence X-ray Topographs and Ray-tracing Simulation in Off-axis 4H-SiC Crystals, ECS Trans. 104 (2021) 157-169.

[15] B. Raghothamachar, Y. Liu, H. Peng, T. Ailihumaer, M. Dudley, F.S. Shahedipour-Sandvik, K.A. Jones, A. Armstrong, A.A. Allerman, J. Han, H. Fu, K. Fu, Y. Zhao, X-ray topography characterization of gallium nitride substrates for power device development, J. Cryst. Growth, 544 (2020) 125709.

[16] T. Zhou, B. Raghothamachar, F. Wu, M. Dudley, Grazing Incidence X-ray Topographic Studies of Threading Dislocations in Hydrothermal Grown ZnO Single Crystal Substrates, MRS Online Proc. Libr. 1494 (2012) 121-126.

[17] M. Dudley, X.R. Huang, W. Huang, Assessment of orientation and extinction contrast contributions to the direct dislocation image, J. Phys. D: Appl. Phys. 32 (1999) A139-A144.

[18] C. Schneider, W. Rasband, K. Eliceiri, NIH Image to ImageJ: 25 years of image analysis, Nat. Methods 9 (2012) 671-675.

[19] A. Authier, Contrast of Dislocation Images in X-Ray Transmission Topography, Adv. X-Ray Anal. 10 (1966) 9-31.

[20] M. Dudley, J. Wu, and G.-D. Yao, Determination of penetration depths and analysis of strains in single crystals by white beam synchrotron X-ray topography in grazing Bragg-Laue geometries, Nucl. Inst. & Meth. B40/41 (1989) 388-392.

[21] H. Peng, T. Ailihumaer, Y. Liu, B. Raghothamachar, X. Huang, L. Assoufid, and M. Dudley, Dislocation contrast on X-ray topographs under weak diffraction conditions, J. Appl. Crystallogr. 54 (2021) 1225-1233.